AIMS Materials Science, 13(1): 148–167.
DOI: 10.3934/matersci.2026009
Received: 14 October 2025
Revised: 29 December 2025
Accepted: 13 January 2026
Published: 02 February 2026

https://www.aimspress.com/journal/Materials

Research article

Green synthesis and use of Fe_2O_3 nanoparticles in the treatment of petroleum effluents by heterogeneous photocatalysis

Clément L. Inkoto[1,2,3,*], Dorothée D. Tshilanda[1], Carlos N. Kabengele[1], Giresse N. Kasiama[1], Christophe Kaki[4], Koto-Te-Nyiwa Ngbolua[2], Waris Kéwouyèmi Chouti[5], Damien S-T. Tshibangu[1], Pius T. Mpiana[1] and Daouda Mama[2]

[1] Laboratory of Natural Substances and Medicinal Chemistry, Department of Chemistry and Industry, Faculty of Science and Technology, University of Kinshasa, Democratic Republic of Congo
[2] Laboratory of Applied Hydrology, National Water Institute (INE), University of Abomey-Calavi, 01 BP: 526 Cotonou, Benin
[3] E-PHYMED Laboratory, Department of Biology, Faculty of Science and Technology, BP 190 Kinshasa XI, University of Kinshasa, Democratic Republic of Congo
[4] Department of Earth Sciences, Faculty of Science and Technology (FAST), University of Abomey-Calavi, Benin
[5] Laboratory of Inorganic and Environmental Chemistry, Faculty of Science and Technology (FAST), University of Abomey-Calavi BP: 4521 Cotonou, Benin

* **Correspondence:** Email: clementinkoto@gmail.com; Tel: +243-812-388-996.

Abstract: The objective of this study was to develop a treatment for petroleum effluents via the use of Fe_2O_3 nanoparticles biosynthesized from extracts of *A. alboviolaceum* leaves as reducing and stabilizing agents. The obtained nanoparticles were characterized via ultraviolet (UV)–visible spectroscopy, X-ray diffraction (XRD), X-ray fluorescence (XRF), energy dispersive X-ray spectroscopy (EDX), Fourier transform infrared spectroscopy (FTIR), and transmission electron microscopy (TEM) to determine their structural and morphological properties. Their photocatalytic activity was evaluated by the degradation of hydrocarbons in petroleum effluents under solar irradiation for 180 min. The results obtained by UV–visible spectroscopy revealed a surface plasmon resonance band at 515 nm. XRD was used to identify the nanoparticles that crystallized in a cubic crystal system (inverse spinel), whereas X-ray fluorescence and EDX were used to identify the chemical composition of the synthesized nanoparticles. The spherical morphology was determined via TEM. The average size of the nanoparticles, 70.43 nm, was determined via ImageJ software. The

hemolytic activity of the biosynthesized nanomaterials revealed that they are not hemotoxic in vitro, and hydrocarbon degradation was observed after 120 min of sunlight irradiation in the presence of Fe_2O_3 nanoparticles, with a high degradation rate (71.9%). Compared with other chemical and physical methods, this study proposes a much simpler and less expensive method for synthesizing nanoparticles. This nanotechnological approach makes it possible to clean up hydrocarbon-contaminated effluents, thereby contributing to environmental protection.

Keywords: *A. alboviolaceum*; green synthesis; Fe_2O_3 nanoparticles; heterogeneous photocatalysis; petroleum effluents

1. Introduction

Water is central to all socioeconomic processes and is universally recognized as a fundamental resource for life and sustainable development [1]. As a key component of the global ecosystem, water supports human health, industrial activities, agriculture, and biodiversity [2]. However, despite its essential role, water resources are increasingly threatened by anthropogenic activities. When water quality is altered, it becomes a major vector of environmental degradation, posing serious risks to ecosystems and public health [3].

Among the various sources of water pollution, petroleum-based activities represent one of the most critical challenges worldwide. The oil industry generates large volumes of wastewater during exploration, extraction, refining, and transportation processes [4]. These effluents, commonly referred to as oily or petroleum wastewater, are often discharged into the environment with insufficient treatment, especially in developing regions [5]. Petroleum effluents typically contain complex mixtures of organic pollutants, including hydrocarbons, phenols, polycyclic aromatic hydrocarbons (PAHs), surfactants, and heavy metals, many of which are toxic, carcinogenic, and poorly biodegradable [6,7]. The presence of these contaminants leads to severe adverse effects on aquatic organisms, soil quality, and human health through bioaccumulation and long-term exposure.

To mitigate petroleum-based water pollution, various conventional treatment methods have been developed, including physical separation, chemical coagulation–flocculation, adsorption, and biological processes [8,9]. Although these methods can be effective under specific conditions, they often suffer from limitations such as incomplete removal of recalcitrant organic compounds, high operational costs, secondary pollution, and sludge generation [10]. Consequently, there is a growing interest in developing alternative and more efficient wastewater treatment technologies that are both environmentally sustainable and economically viable.

In this context, heterogeneous photocatalysis has emerged as a promising advanced oxidation process for wastewater treatment. This technique relies on the generation of reactive oxygen species under light irradiation, enabling the degradation and mineralization of persistent organic pollutants into harmless end products such as carbon dioxide and water [9]. Photocatalysis offers several advantages, including high degradation efficiency, minimal chemical consumption, and the potential use of solar energy, making it particularly attractive for environmental remediation applications [11].

Among the various photocatalysts investigated, Fe_2O_3 has attracted significant attention due to its low toxicity, natural abundance, chemical stability, and suitable band gap for visible light absorption. These properties make Fe_2O_3 an environmentally benign and cost-effective material for photocatalytic

applications. Previous studies have demonstrated the effectiveness of Fe_2O_3 nanoparticles in the degradation of organic pollutants such as dyes, phenolic compounds, and petroleum-derived contaminants [10]. However, the photocatalytic performance of Fe_2O_3 is strongly influenced by its particle size, morphology, surface chemistry, and synthesis route.

Conventional synthesis methods for Fe_2O_3 nanoparticles, including sol–gel, hydrothermal, co-precipitation, and thermal decomposition techniques, often involve the use of organic solvents, high energy consumption, and hazardous chemical reagents [10,12]. These factors limit their environmental sustainability and large-scale applicability. In response to these concerns, green synthesis approaches have gained increasing interest in recent years. Green synthesis utilizes biological resources, such as plant extracts, microorganisms, or biopolymers, as reducing and stabilizing agents, thereby minimizing the use of toxic chemicals and reducing environmental impact [13].

Plant-mediated green synthesis is particularly attractive due to its simplicity, low cost, and scalability. Plant extracts are rich in secondary metabolites such as polyphenols, flavonoids, tannins, and alkaloids, which play a crucial role in the reduction of metal ions and stabilization of nanoparticles. Among various plant species, *Aframomum alboviolaceum* has been reported to be non-toxic and rich in bioactive compounds with strong reducing and capping abilities [14]. Despite the growing number of studies on green-synthesized iron oxide nanoparticles, their application in the photocatalytic treatment of real petroleum effluents remains limited, and the relationship between green synthesis routes and photocatalytic efficiency is still insufficiently explored [15].

Therefore, the present study aims to develop an eco-friendly and efficient treatment strategy for petroleum effluents using Fe_2O_3 nanoparticles biosynthesized from *A. alboviolaceum* leaf extracts. The novelty of this work lies in the combined use of a green synthesis approach and heterogeneous photocatalysis for the remediation of petroleum-contaminated wastewater. This study contributes to the advancement of sustainable nanomaterials and highlights the potential of plant-based synthesized Fe_2O_3 nanoparticles as effective photocatalysts for environmental applications.

2. Materials and methods

2.1. Materials

The leaves of *A. alboviolaceum* (Ridley) K. Schum. used in this study for the synthesis of Fe_2O_3 nanoparticles (NPs), were collected on June 3, 2024, in the Mitendi savanna located in the commune of Mont-Ngafula in Kinshasa, DRC. After harvesting, a sample of the plant was taken for identification to the Herbarium of the National Institute for Agronomic Studies and Research (INERA) located at the Faculty of Sciences of the University of Kinshasa (UNIKIN). These leaves were dried at ambient temperature (±27 °C) in the Laboratory of Natural Substances and Medicinal Chemistry (LASCHIMED) for two weeks and then ground to obtain a fine powder. The blood used in this study was provided by the Mont-amba Hospital Center located in the commune of Lemba in Kinshasa. To be included in this study, blood had to come from a healthy subject who had given their consent prior to collection.

2.2. Methods

2.2.1. Preparation of aqueous extract

Twenty grams of *A. alboviolaceum* leaf powder was macerated in distilled water for 24 h and then filtered through filter paper (Whatman No. 42) to obtain the aqueous extract, which was used as a reducing agent and stabilizer in the synthesis of nanoparticles.

2.2.2. Phytochemical screening

The different groups of secondary metabolites that act as reducing agents and stabilizers were identified via conventional phytochemical screening and thin-layer chromatography, a technique based on the observation of spot colors as previously described by Ngbolua et al. [16] and Inkoto et al. [17].

2.2.3. Preparation of Fe_2O_3 NPs from plant extracts

The experimental procedure previously described by Kabengele et al. [18] and Kasiama et al. [19] was used for the biogenic synthesis of Fe_2O_3 nanoparticles with slight modifications. Briefly, 100 mL of a 0.01 N Fe_2SO_4 solution was mixed with 20 mL of the aqueous extract of *A. alboviolaceum* leaves under thermal agitation at 80 °C and 1000 rpm. After 120 min of stirring, the change in color of the solution from yellow to dark green indicated the beginning of the precipitation of metal ions in the form of nanoparticles. The obtained nanoparticle precipitate was centrifuged at 4000 rpm, washed three times with distilled water to remove impurities, calcined at 200 °C in an oven for 4 h, and stored at room temperature for characterization. A 0.01 N NaOH solution was used to vary the pH of the medium.

2.2.4. Characterization of Fe_2O_3 NPs

The surface plasmon resonance of the synthesized Fe_2O_3 nanoparticles was studied by performing a wavelength scan ranging from 200 to 700 nm via UV–vis (UV–visible spectrophotometer, Jenway 7615). Crystallographic analysis of the synthesized nanoparticles was performed via an X-ray diffractometer (PHYWE 4.0) with a Cu-Kα source ($\lambda = 1.540596$ Å) at 2θ angles between 20 and 90°. The chemical functions of the molecules used for particle reduction and stabilization were determined via Fourier transform infrared spectroscopy (FTIR) spectrophotometer (Cary 630 FTIR). Transmission electron microscopy (TEM) was used to characterize the morphology of the nanoparticles. The average particle size was evaluated via ImageJ software. The elemental composition of the particles was determined via energy dispersive X-ray spectroscopy (EDX) and X-ray fluorescence (XRF).

2.2.5. Properties of the Fe_2O_3 NPs

2.2.5.1. Adsorption and photocatalytic activity

The adsorption and photocatalytic activities of the nanoparticles were evaluated by degrading an aqueous solution containing petroleum pollutants at room temperature under agitation. To do this, 100 mL of water polluted with 20% hydrocarbons was mixed with 10 mg of nanocatalyst under agitation in the

absence of light for 180 min to achieve a homogeneous distribution of the catalyst in the medium and reach adsorption-desorption equilibrium on the surface of the nanoparticles. Every 60 min, an aliquot was taken and measured via a UV–visible spectrophotometer. The mixture was then irradiated with sunlight for 120 min, and after every 60 min, an aliquot (2 mL) was taken and analyzed with an UV–visible spectrophotometer scanning between 200 and 400 nm. The rate of hydrocarbon degradation was determined (Figure 1).

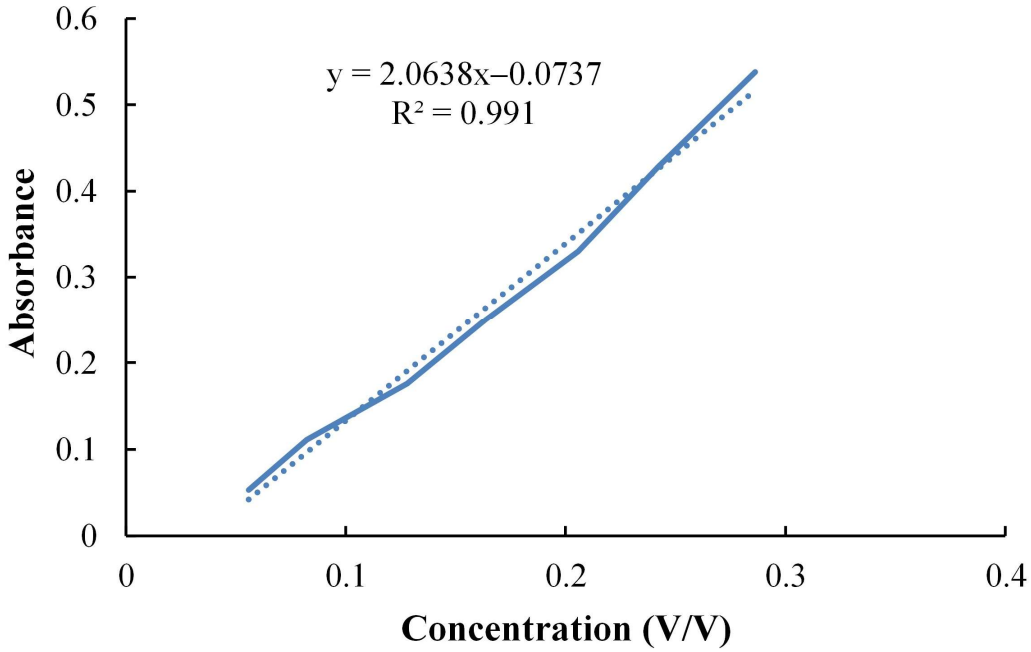

Figure 1. Calibration curve for the gasoline used.

2.2.5.2. Hemolytic activity of the Fe_2O_3 NPs

Certain compounds may pose a risk of hemolysis to red blood cells. Determining the hemolytic effect is one of the most commonly used tests for studying the interaction of nanomaterials with blood components (red blood cells). In this study, the hemolytic power of the nanoparticles in vitro was evaluated according to the experimental protocol previously described by Chen et al. [20] and Gbolo et al. [21].

3. Results and discussion

3.1. Conventional phytochemical screening and Thin-Layer Chromatography (TLC)

The results of conventional phytochemical screening revealed several phytochemical groups, including phenolic acids, flavonoids, tannins, alkaloids, coumarins, iridoids, saponins, anthocyanins, and terpenes. Thin-layer chromatography confirmed the presence of anthocyanins (Figure 2a), iridoids (Figure 2b), coumarins (Figure 2c), and phenolic acids (Figure 2d) in the leaf extract of this plant. These results are similar to those of Bongo et al. [22], Djeussi et al. [23], and Inkoto et al. [17] in the leaves of *A. alboviolaceum*. The presence of these compounds, such as phenolic acids,

flavonoids, and terpenes, which act as both reducing agents and stabilizers, justifies the use of this plant extract in the synthesis of nanoparticles [24].

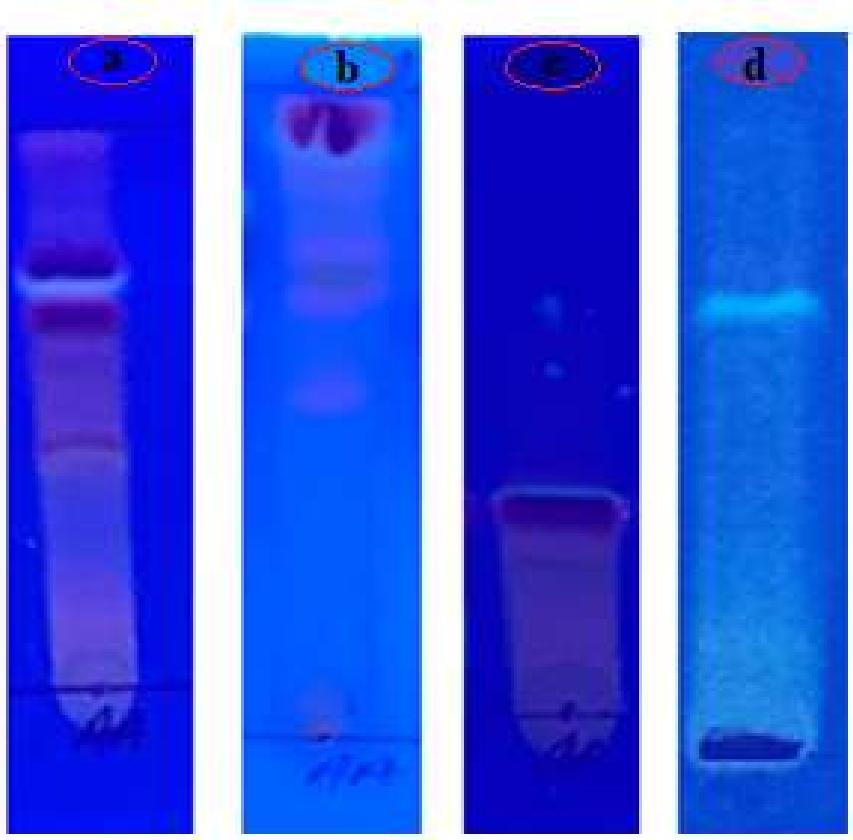

Figure 2. Chromatogram showing the detection of (a) anthocyanins, (b) iridoids, (c) coumarins, and (d) phenolic acids.

3.2. Synthesis of Fe_2O_3 NPs

Figure 3 shows the synthesis of Fe_2O_3 NPs in solution from extracts of *A. alboviolaceum* leaves.

Figure 3. Synthesis of Fe_2O_3 NPs in solution from extracts of *A. alboviolaceum* leaves.

As shown in Figure 3a, the solution initially has a yellow color when the precursor salt (Fe_2SO_4) and the extract of *A. alboviolaceum* are mixed. After 30 min of heating at 80 °C, the color changes from yellow to green (Figure 3b), indicating the start of nanoparticle formation in solution. At this

stage, stabilization has not yet occurred; this is the reduction and nucleation phase, which involves reducing compounds contained in the plant extract, such as phenolic acids, flavonoids, and terpenes [24,25]. After 30 min of thermal agitation at 80 °C, we observed a color change from green to dark green, almost blackish (Figure 3c). This color (dark green) persisted for up to 120 min of reaction under thermal agitation, confirming the stabilization of the nanoparticles in solution. Previous studies have shown that secondary metabolites (polyphenols, saponins, flavonoids, condensed tannins, etc.) in plant extracts are responsible for reducing iron (III) ions to iron oxide NPs and stabilizing them [26,27].

3.3. Characterization of nanoparticles

3.3.1. Characterization by UV–visible spectroscopy

Since the absorption wavelength is characteristic of nanoparticles, confirming the presence of nanoparticles by the presence of their characteristic band or surface plasmon resonance band is important. The figures below show the UV–visible spectra of the mixture of precursor salt and *A. alboviolaceum* extract at time t = 0 (Figure 4) and the UV–visible spectrum of the Fe_2O_3 NPs synthesized from *A. alboviolaceum* extracts after 120 min (Figure 5). A comparison of Figures 4 and 5 reveals that for the same solution, after 120 min, a characteristic band between 470 and 550 nm appears in Figure 5, indicating the presence of iron oxide nanoparticles. This band indicates the surface plasmon resonance of iron oxide nanoparticles, with a maximum at approximately 515 nm.

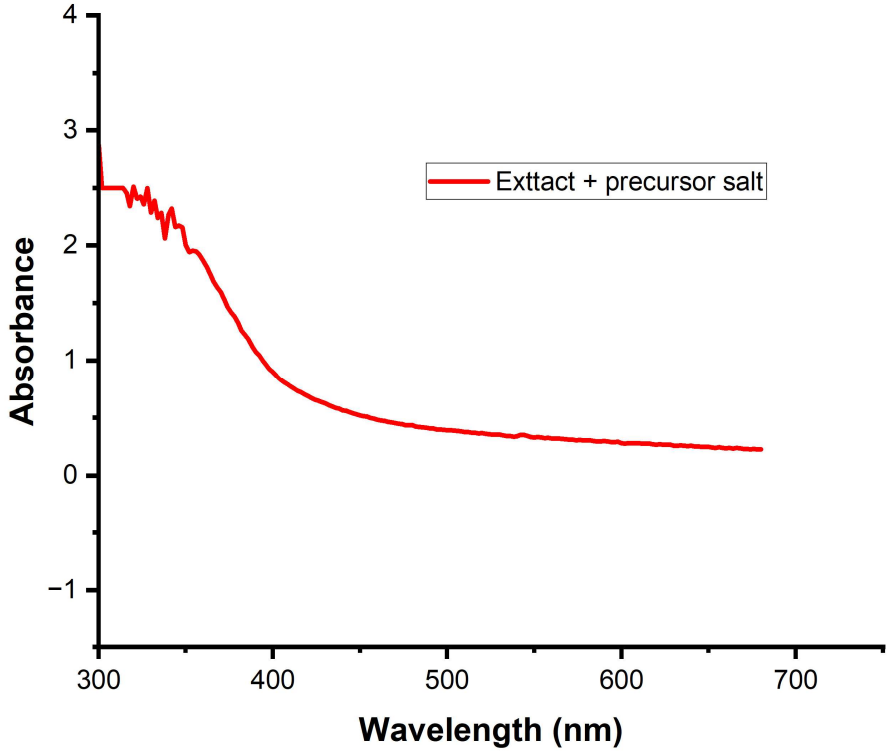

Figure 4. UV–visible spectrum of the mixture of precursor salt and *A. alboviolaceum* extract at time t = 0.

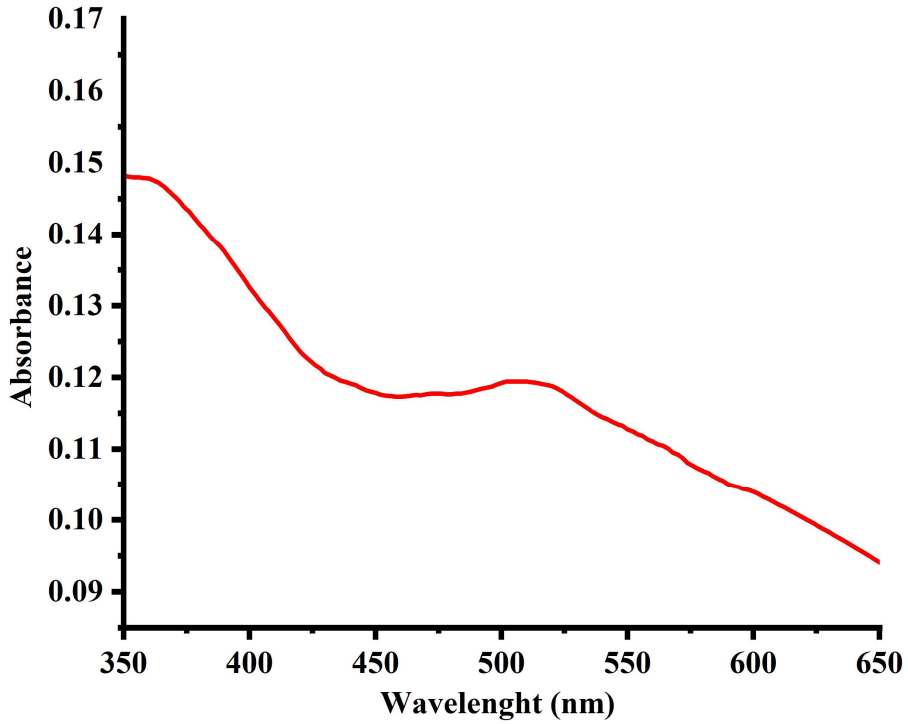

Figure 5. UV–visible spectra of Fe_2O_3 NPs synthesized from extracts of *A. alboviolaceum.*

Figure 6 shows that, after extrapolating the curve, the energy of the doped Fe_2O_3 gap is 2.4 eV. This energy gap is similar to the typical values of the Fe_2O_3 optical gap, which ranges from 2.0 to 2.4 eV.

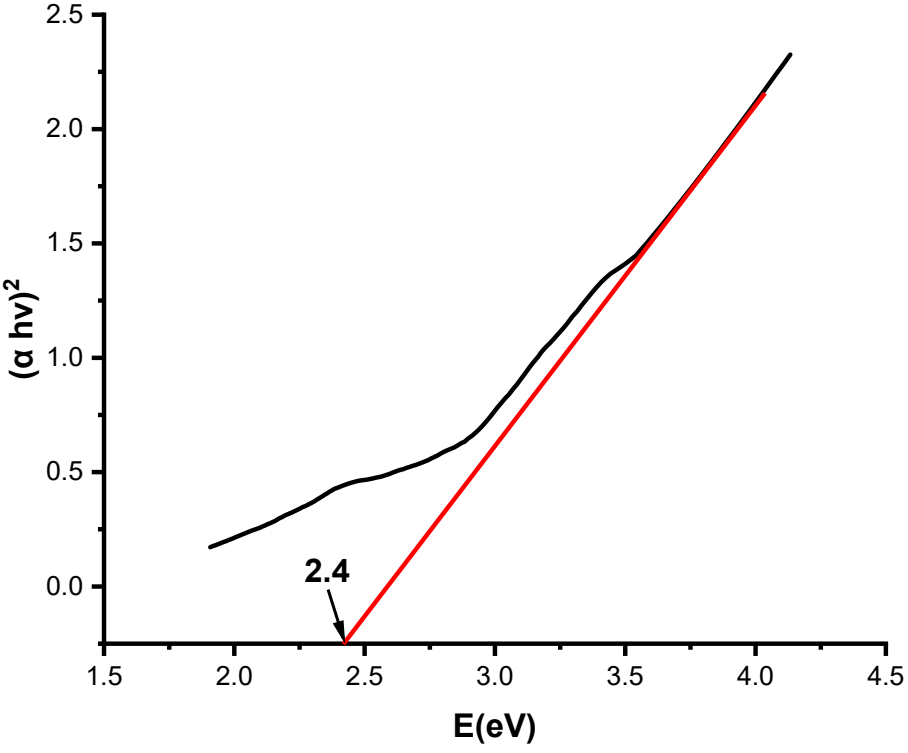

Figure 6. Variation in $(\alpha h\nu)^2$ as a function of the energy of the Fe_2O_3 NPs.

3.3.2. Characterization by X-ray diffraction (XRD)

To determine the crystal structure, lattice parameters, crystallite size, and chemical composition of the synthesized Fe_2O_3 nanoparticles, XRD data were recorded via a PHYWE 4.0 X-ray spectrometer. The results obtained are shown in Figure 7 below.

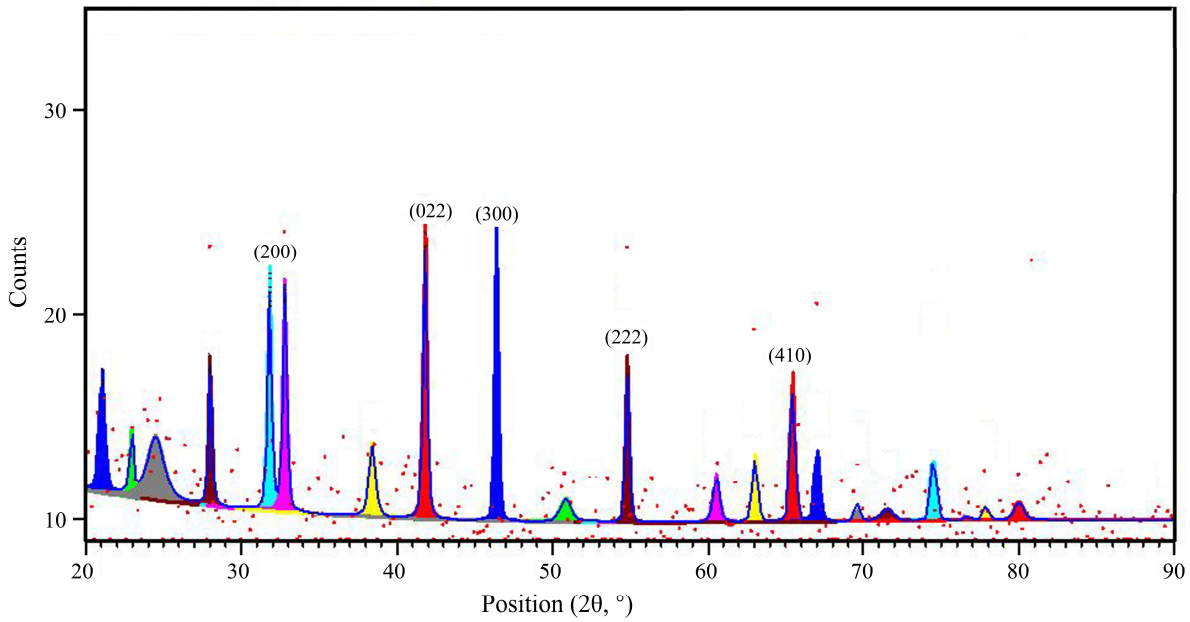

Figure 7. XRD spectrum of synthesized Fe_2O_3 NPs.

Five characteristic peaks associated with the reticular planes (200), (022), (300), (222), and (410) appeared at the following 2θ positions: 31.7894° (66.74%), 41.7721° (89.75%), 46.3657° (100%), 54.7648° (70.68%), and 65.3708° (93.46%), respectively (Figure 7). The spectrum in Figure 7 shows that the iron oxide nanoparticles crystallized in a face-centered cubic system (γ-Fe_2O_3) with a lattice parameter of a = 0.8326 Å. Furthermore, the characteristic angles of this material match the JCPDS standard card No. 39-1346, confirming that it is maghemite (γ-Fe_2O_3). Notably, the additional low-intensity peaks observed in this spectrum were attributed to the presence of different oxide residues (Fe_3O_4 or α-Fe_2O_3), amorphous phases, or biomass products (adsorbed organic compounds). The theoretical size was estimated from this spectrum. After calculation and statistical processing, the average size of the crystallites obtained via the Debye-Scherrer equation was 47 ± 6 nm. These results confirm the success of the synthesis and demonstrate that the particles obtained do indeed have the expected nanometric dimensions. Thus, the extract of *A. alboviolaceum* is an effective reducing and stabilizing agent for the production of maghemite nanoparticles.

3.3.3. Characterization by fluorescence and EDX

The X-ray fluorescence (Figure 8) and energy dispersive X-ray (Figure 9) spectra shown below reveal the composition of the synthesized nanoparticles. The X-ray fluorescence spectrum confirmed the presence of the metal used (Fe-Kα). Moreover, the EDX spectrum revealed that the synthesized nanoparticles are composed of both iron and oxygen, with percentages of 69.13% and 30.60% for iron

and oxygen, respectively. However, the presence of a small percentage of carbon (6.08%) could be due to the phytochemical compounds acting as a coating. These results confirm that the synthesized particles are iron oxide particles.

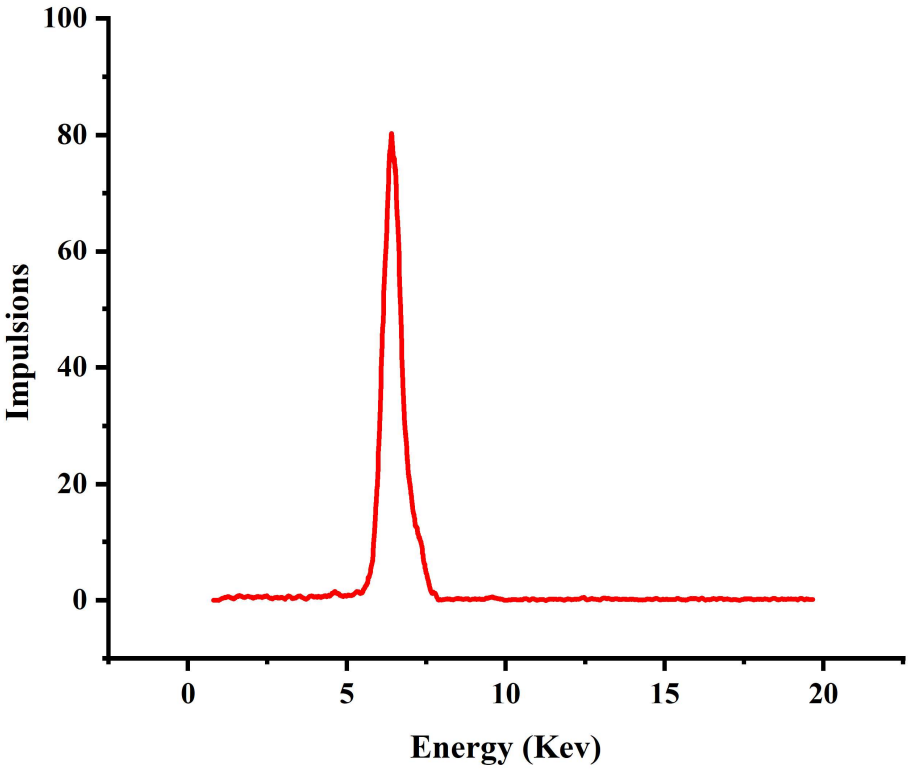

Figure 8. Fluorescence spectrum of synthesized Fe_2O_3 nanoparticles.

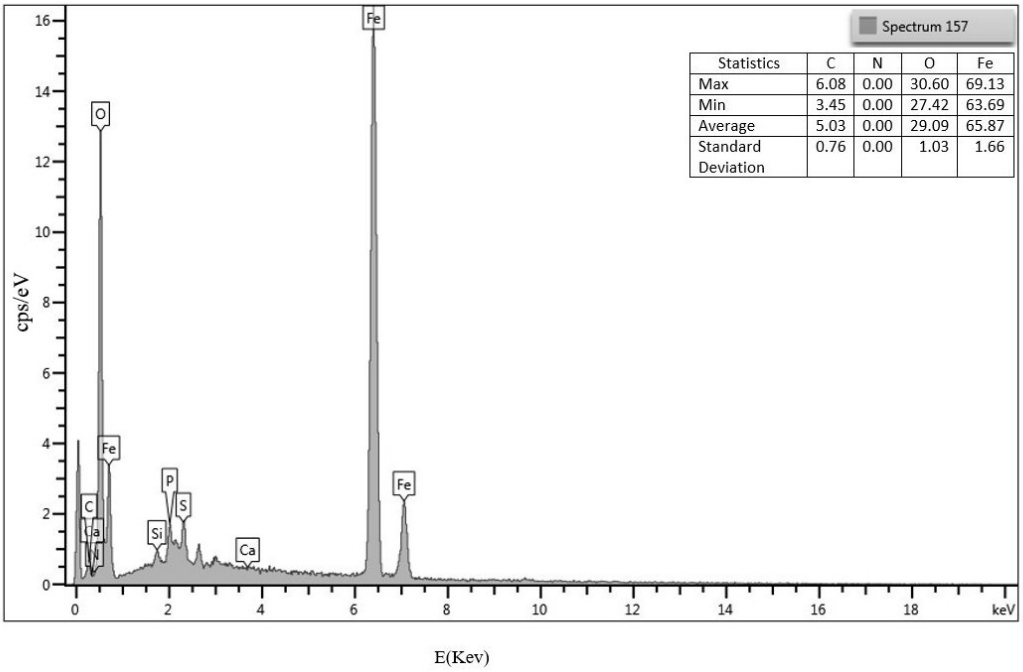

Figure 9. EDX spectrum of synthesized Fe_2O_3 nanoparticles.

3.3.4. Characterization by FTIR

Secondary metabolites play a key role in the green synthesis of metal nanoparticles from plants. To determine the functions of the molecules used for reduction and stabilization in this synthesis, an FTIR spectrum was obtained via a Fourier transform infrared spectrophotometer, Cary 630 FTIR. Figure 10 shows the FTIR spectrum of the synthesized nanoparticles.

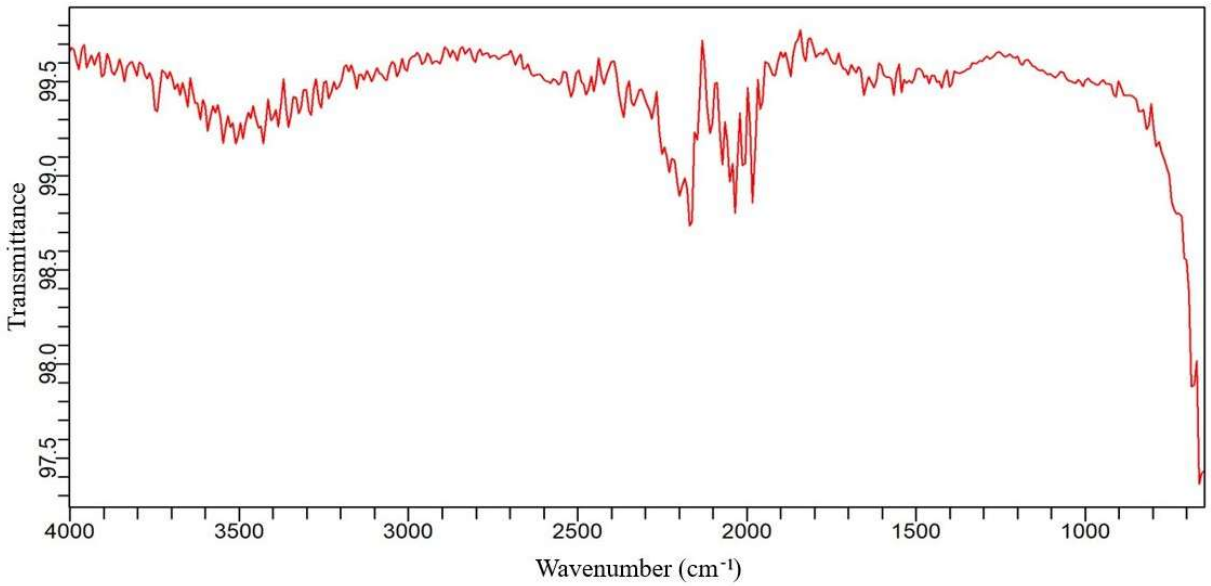

Figure 10. FTIR spectrum of synthesized Fe_2O_3 NPs.

As shown in Figure 10, the characteristic bands between 1600 and 1700 cm^{-1} are attributed to the stretching vibrations of the C=O bonds of carbonyls. The peak at approximately 2035 cm^{-1} is associated with the metal complex, including iron carbonyl (Fe–CO) and iron-complexed nitrile (Fe–C≡N). However, the peak at approximately 3500 cm^{-1} is characteristic of O–H stretching vibrations, which could result from the presence of phenolic compounds in the extract of the plant used. There is a strong peak at approximately 650 cm^{-1}, which can be attributed to the Fe–O stretching vibration [28].

3.3.5. Characterization by TEM

Morphology is one of the key parameters in nanoparticle synthesis, as it directly influences the subsequent physical and chemical properties of synthesized nanometric materials [29]. Figure 11 shows a TEM image of the Fe_2O_3 NPs.

As shown in Figure 11, the TEM image clearly shows a predominantly spherical particle morphology on a scale of 100 nm. These results, concerning the morphology of the nanoparticles synthesized in this study, are similar to the conclusions of Abdul et al. [30], who reported the formation of iron oxide nanoparticles synthesized from *Phoenix dactylifera* seed extract. The average size of the Fe_2O_3 nanoparticles synthesized from *A. alboviolaceum* leaf extract, as estimated from TEM micrographs via ImageJ and Origin software, was 70.43 nm (Figure 12), confirming the formation of particles smaller than 100 nm.

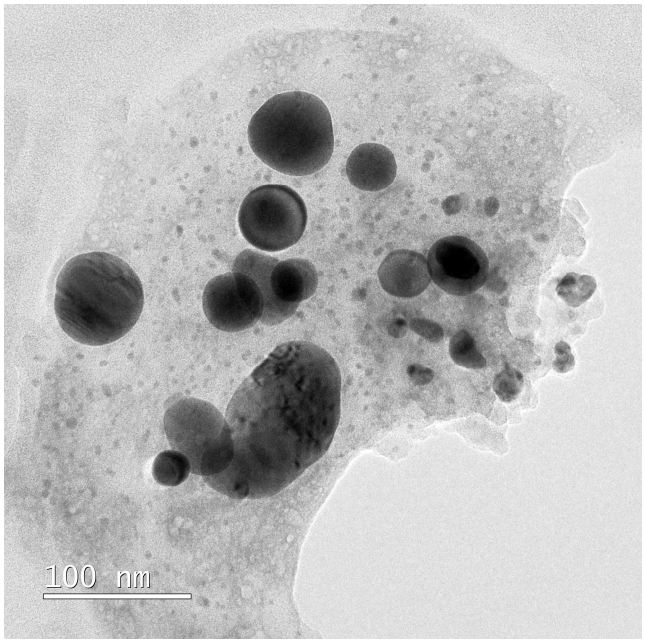

Figure 11. TEM image of Fe_2O_3 NPs synthesized from extracts of *A. alboviolaceum* leaves.

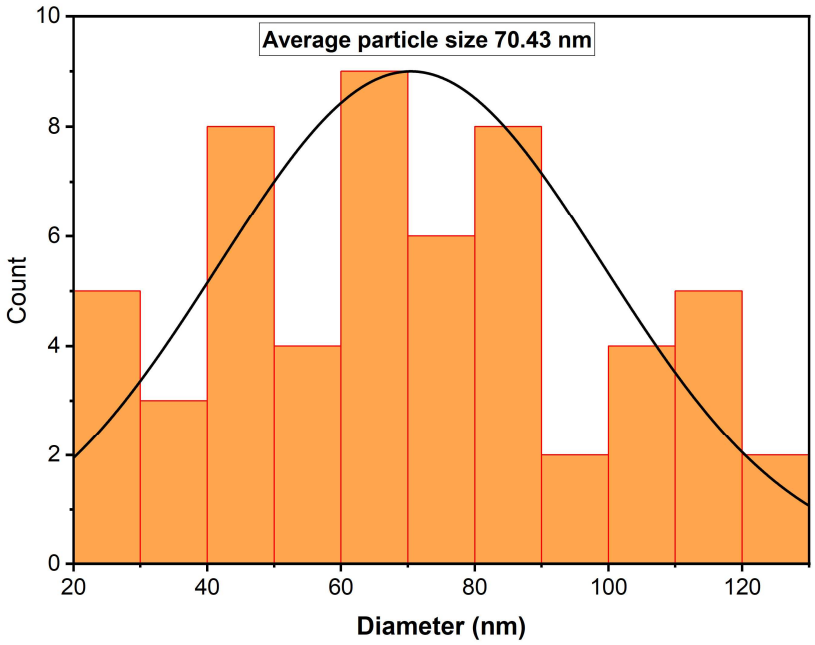

Figure 12. Distribution of the average size of the Fe_2O_3 nanoparticles.

3.4. Application of Fe_2O_3 NPs in the degradation of polluted water

The photocatalytic properties of the biosynthesized Fe_2O_3 NPs were evaluated using water polluted with super gasoline, whose visible UV spectrum showed a maximum band at approximately 280 nm. In this study, the polluted water solution alone was used as a negative control after solar irradiation at well-defined time intervals. Figure 13 shows that sunlight does not cause HC degradation, so the photolysis mechanism was ruled out.

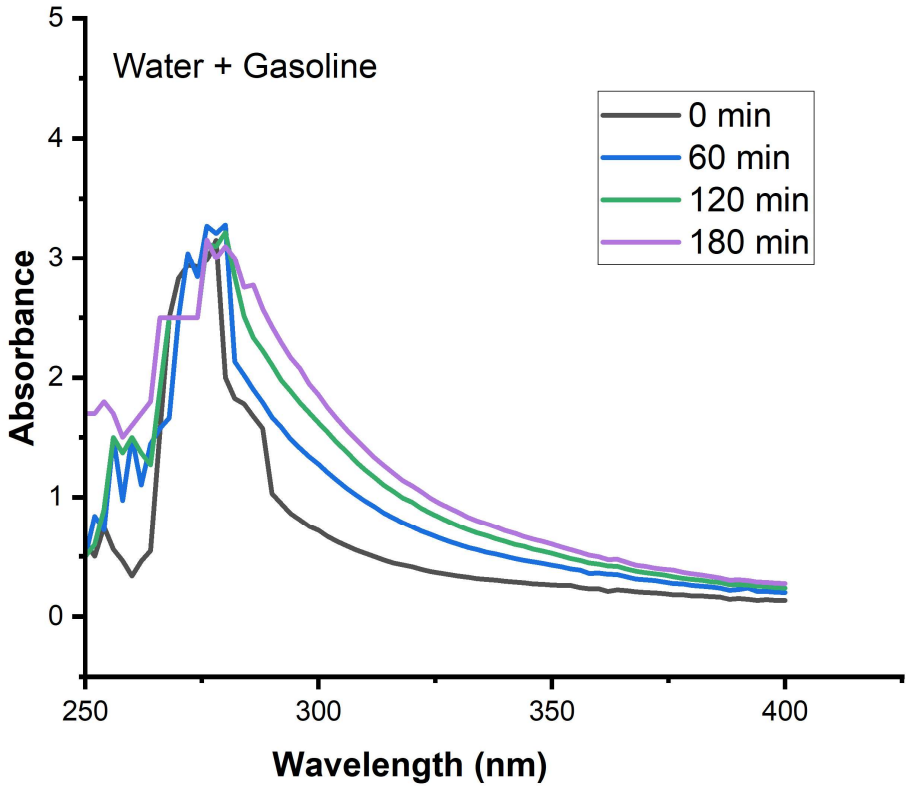

Figure 13. Exposure of polluted water solutions to sunlight.

Next, the Fe_2O_3 NPs were placed in contact with the polluted water while stirring at 1,000 rpm in the dark, and the absorbances were determined at different times to evaluate the adsorption activity on the surface of the nanoparticles. The results shown in Figure 14 below indicate that the NPs adsorb a large proportion of the hydrocarbons, with a maximum adsorption rate of approximately 17.1%. This adsorption could be attributed to the various defects on the surface of the synthesized nanoparticles, which generate highly attractive sites that strongly promote adsorption [31].

After the mixture of the polluted solution and nanoparticles was exposed to light, the results shown in Figure 15 revealed significant photocatalytic activity, with the Fe_2O_3 NPs degrading approximately 71.9% of the hydrocarbons after 180 min of exposure. UV–visible spectroscopy was used to monitor the photocatalytic degradation of hydrocarbons over time, and the results are presented in Figure 15 below.

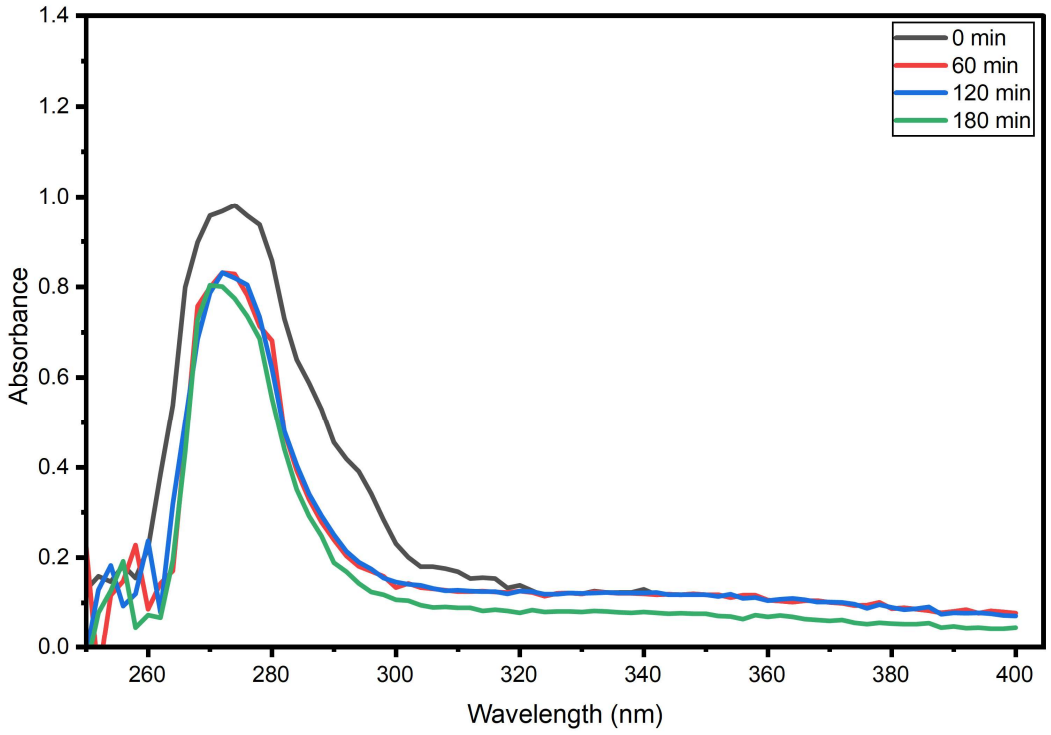

Figure 14. Adsorption of hydrocarbons on the surface of Fe_2O_3 nanoparticles.

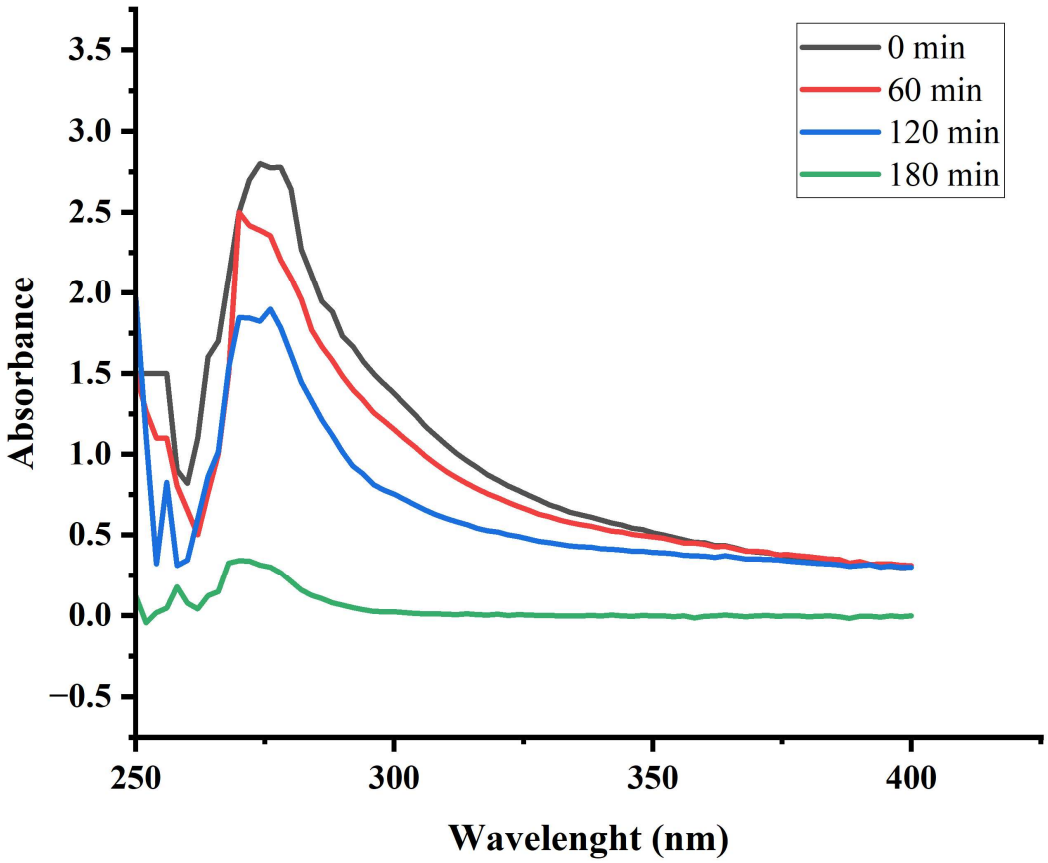

Figure 15. Photocatalytic degradation of gasoline by Fe_2O_3 NPs.

In fact, Fe_2O_3 NPs behave like semiconductors capable of absorbing visible light and generating electron/hole pairs on their surfaces. These charges react with water and oxygen to produce reactive oxygen species (ROS), such as hydroxyl radicals ($OH^{\bullet}$) and superoxide anion radicals. These ROS have the intrinsic ability to degrade all types of pollutants [32,33]. In a study conducted by Akintayo et al. [34] on the use of iron oxide NPs in the treatment of synthetic oil wastewater, a maximum degradation rate of approximately 89.0% was found after 60 min of irradiation. Notably, in this study, the authors irradiated the iron oxide NPs with a UV–visible lamp at 254 nm, and these NPs were synthesized via a chemical reduction method. This may explain the difference in performance compared with our results. Bolade et al. [35] reported degradation rates greater than or equal to 93% with FeNPs alone and up to 99%–100% when they activated persulfate within a few days, owing to highly efficient radical oxidation, but with the need for an additional oxidant. Muthukumar et al. [36] combined bacteria, biosurfactants, and FeNPs to achieve 82% yield in 20 days, which is a gentler but much slower bioremediation process. Thus, our process is faster than microbial bioremediation but slightly less complete than FeNP + persulfate oxidative catalysis and could be optimized to further improve the final yield while limiting the environmental impact.

Figure 16 illustrates the temporal evolution of free hydrocarbon concentration in the reaction medium as a function of irradiation time.

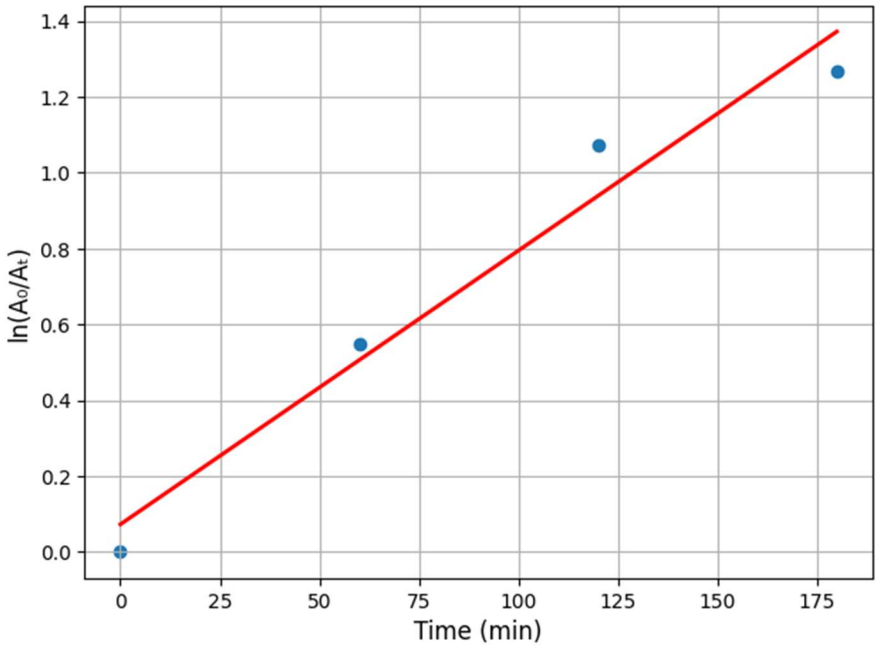

Figure 16. Pseudo-first-order kinetic plot for photocatalytic degradation of petroleum effluents over Fe_2O_3 nanoparticles.

The kinetic behavior of petroleum effluent degradation over Fe_2O_3 nanoparticles was evaluated by plotting $\ln(A_0/A_t)$ as a function of irradiation time. The obtained linear relationship confirms that the photocatalytic process follows pseudo-first-order kinetics, consistent with the Langmuir–Hinshelwood model typically observed in heterogeneous photocatalytic systems [37]. Moreover, the progressive increase of $\ln(A_0/A_t)$ with irradiation time indicates an efficient and continuous removal of petroleum-derived organic contaminants. The strong linearity between experimental data and the fitted regression line suggests that the reaction rate is predominantly governed by surface-mediated redox

reactions involving photoinduced charge carriers and reactive oxygen species, notably hydroxyl radicals and superoxide anions.

3.5. Evaluation of the hemolytic activity of the Fe_2O_3 NPs

The size and morphology of nanoparticles completely affect their physicochemical properties; hence, their cytotoxicity needs to be studied. The results of the hemolytic effects of the NPs synthesized from *A. alboviolaceum* extracts on blood cells are shown in Table 1 below.

Table 1. Hemolytic effect of the biosynthesized nanoparticles on red blood cells.

Sample	Hemolysis (%)
Fe_2O_3 NPs	1.94
Positive control	100.00
Negative control	0.00

Cytotoxicity was assessed using erythrocytes as a biological model. NPs are considered cytotoxic when, at 100 µg/mL, the hemolysis rate is ≥25% [12,18,38]. In this study, Fe_2O_3 NPs synthesized from *A. alboviolaceum* extracts at 1000 µg/mL had a hemolysis percentage of 1.94% (less than 25%). This result indicates that the synthesized nanoparticles are less hemolytic.

4. Conclusions

The aim of this work was to develop a treatment for petroleum effluents via the use of Fe_2O_3 nanoparticles biosynthesized from extracts of *A. alboviolaceum* leaves as reducing and stabilizing agents. The obtained Fe_2O_3 nanoparticles have morphological and structural properties favorable for photocatalytic activation under visible light. The results obtained by UV–visible spectroscopy revealed a surface plasmon resonance band at 515 nm. XRD identified the nanoparticles as having crystallized in a cubic crystal system (inverse spinel), whereas X-ray fluorescence and EDX identified the chemical composition of the synthesized nanoparticles. The spherical morphology was determined via TEM. Moreover, the average size of the 70.43 nm nanoparticles was determined via ImageJ software. The hemolytic activity of the biosynthesized nanomaterials revealed that they are not hemotoxic in vitro, and hydrocarbon degradation was observed after 120 min of sunlight irradiation in the presence of Fe_2O_3 nanoparticles, with a high degradation rate (71.9%). The results obtained in this study confirm the potential of the Fe_2O_3 NPs biosynthesized from *A. alboviolaceum* extract as effective catalysts for the decontamination of hydrocarbon-polluted water, which is consistent with the logic of sustainable development and the valorization of local natural resources. Compared with other chemical and physical methods, this study proposes a much simpler and less expensive method for synthesizing nanoparticles. It would therefore be desirable to conduct a study on the stability of nanoparticles for reuse during several photocatalysis cycles.

Use of AI tools declaration

The authors declare they have not used Artificial Intelligence (AI) tools in the creation of this article.

Acknowledgments

This research was supported by the African Center of Excellence for Water and Sanitation at the National Water Institute (INE), University of Abomey-Calavi in Benin. The authors are grateful to the Laboratory of Natural Substances and Medicinal Chemistry (LASHIMED) of the Department of Chemistry and Industry, University of Kinshasa, for the facilities made available to us to make this study possible.

Author contributions

Clément L. Inkoto: writing–original draft and formal analysis; Carlos N. Kabengele and Giresse N. Kasiama: formal analysis and investigation; Waris Kéwouyèmi Chouti: conceptualization; Christophe Kaki: investigation; Dorothée D. Tshilanda: investigation; Koto-te-Nyiwa Ngbolua: conceptualization; Pius T. Mpiana: conceptualization; Daouda Mama and Damien S-T. Tshibangu: methodology.

Conflict of interest

The authors declare no conflict of interest.

References

1. Benosman Née Bengrine A (2016) Contribution à l'étude de la rétention des polluants par des réseaux de polymères. *Thèse de doctorat*, Université Abou-Bekr Belkaid–Tlemcen, Algérie. Available from: https://dspace.univ-tlemcen.dz/handle/112/15224.
2. Dezani C (2020) Photocatalyse hétérogène en réacteurs ouverts pour la gestion de la ressource solaire: expérimentation sur différents médias et modélisation. *Thèse de doctorat*, Université de Perpignan, France. Available from: https://theses.hal.science/tel-03105379v1/file/These_Chloe_Dezani_2020.pdf.
3. Amiard JC (2011) Les risques chimiques environnementaux: Méthodes d'évaluation et impacts sur les organismes. *Lavoisier*, Paris, France. Available from: https://www.sudoc.fr/232749213.
4. Zhuang Y, Zhu Q, Li G, et al. (2022) Photocatalytic degradation of organic dyes using covalent triazine-based framework. *Mater Res Bull* 146: 111619. https://doi.org/10.1016/j.materresbull.2021.111619
5. Fatima Z, Loubna H (2016) Traitement des eaux contaminées par les produits pétroliers: cas du complexe de Rhourde-Nouss. *Mémoire de master*, Université Larbi Ben M'hidi, Oum El Bouaghi, Algérie.
6. Varjani SJ (2017) Microbial degradation of petroleum hydrocarbons. *Bioresource Technol* 223: 277–286. https://doi.org/10.1016/j.biortech.2016.10.037

7. Ite AE, Ibok UJ, Ite MU, et al. (2013) Petroleum exploration and production: Past and present environmental issues in the Nigeria's Niger Delta. *Am J Environ Prot* 4: 78–90. https://doi.org/10.12691/env-1-4-2
8. Msaboue ML, Merragueb AK (2022) Traitement des effluents de l'industrie pétrolière par procédé membranaire. *Mémoire de master*, Université de Tissemsilt, Algérie.
9. Fujishima A, Zhang X, Tryk DA (2008) TiO_2 photocatalysis and related surface phenomena. *Surf Sci Rep* 63: 515–582. https://doi.org/10.1016/j.surfrep.2008.10.001
10. Ahmad W, Joshi HC, Pandey S, et al. (2022) An overview of green methods for Fe_2O_3 nanoparticle synthesis and their applications. *Int Nano Lett* 13: 2. https://doi.org/10.1007/s40089-022-00386-w
11. Sibhatu AS, Weldegebrieal KG, Sgaradevan S, et al. (2022) Photocatalytic activity of CuO nanoparticles for organic and inorganic pollutants removal in wastewater remediation. *Chemosphere* 299: 134623. https://doi.org/10.1016/j.chemosphere.2022.134623
12. Mittal AK, Chisti Y, Banerjee UC (2013) Synthesis of metallic nanoparticles using plant extracts. *Biotechnol Adv* 31: 346–356. https://doi.org/10.1016/j.biotechadv.2013.01.003
13. Aisida SO, Ugwu K, Nwanya AC, et al. (2021) Dry *Gongronema latifolium* aqueous extract mediated silver nanoparticles by one-step in-situ biosynthesis for antibacterial activities. *Surf Interfaces* 24: 101116. https://doi.org/10.1016/j.surfin.2021.101116
14. Inkoto CL, Ngbolua KN, Kilembe JT, et al. (2021) A mini review on the phytochemistry and pharmacology of *Aframomum alboviolaceum* (Zingiberaceae). *South Asian Research J Nat Prod* 4: 24–35. Available from: https://www.tropicalplantresearch.com/download/135/24.pdf.
15. Khan MA, Ahmed M, Abu-Hussien SH, et al. (2025) Green synthesis of iron oxide nanoparticles (Fe_2O_3-NPs) from *Citrus limetta* agrowaste for biological and photocatalytic applications. *Sci Rep* 15: 33107. https://doi.org/10.1038/s41598-025-17750-3
16. Ngbolua KN, Shetonde OM, Inkoto CL, et al. (2016) Ethno-botanical survey of plant species used in traditional medicine in Kinshasa city (Democratic Republic of the Congo). *Trop Plant Res* 3: 413–422.
17. Inkoto CL, Bongo GN, Kapepula PM, et al. (2017) Microscopic features and chromatographic fingerprints of selected Congolese medicinal plants. *Emerg Life Sci Res* 4: 1–10. https://doi.org/10.31783/elsr.2018.410110
18. Kabengele CN, Kasiama GN, Ngoyi EM, et al. (2023) Biogenic synthesis, characterization and effects of Mn–CuO composite nanocatalysts on methylene blue photodegradation and human erythrocytes. *AIMS Mater Sci* 10: 356–369. https://doi.org/10.3934/matersci.2023019
19. Kasiama GN, Kabengele CN, Kilembe JT, et al. (2023) Green synthesis, characterization and evaluation of biological activities of Ag–MnO nanocomposites from *Cyttaranthus congolensis*. *Diyala J Eng Sci* 16: 24–36. https://doi.org/10.24237/djes.2023.16303
20. Chen LQ, Li F, Ling J, et al. (2015) Nanotoxicity of silver nanoparticles to red blood cells: Size-dependent adsorption, uptake, and hemolytic activity. *Chem Res Toxicol* 28: 501–509. https://doi.org/10.1021/tx500479m
21. Gbolo BZ, Ciala BN, Ngbolua JKN, et al. (2022) Profilage phytochimique par chromatographie sur couche mince haute performance d'extraits de flavonoïdes totaux du Drepanoalpha® et évaluation de leur activité antidrépanocytaire *in vitro*. *Ann Afr Med* 16: e4882–e4898. https://doi.org/10.4314/aamed.v16i1.3

22. Bongo G, Inkoto C, Masengo C, et al. (2017) Antisickling, antioxidant and antibacterial activities of *Aframomum alboviolaceum*, *Annona senegalensis* and *Mondia whitei*. *American J of Lab Med* 2: 52–59. https://doi.org/10.11648/J.AJLM.20170204.13
23. Djeussi DE, Noumedem JAK, Seukep JA, et al. (2013) Antibacterial activities of selected edible plant extracts against multidrug-resistant gram-negative bacteria. *BMC Complement Altern Med* 13: 164. https://doi.org/10.1186/1472-6882-13-164
24. Singh PK, Bhardwaj K, Dubey P, et al. (2015) UV-assisted size sampling and antibacterial screening of *Lantana camara* leaf extract synthesized silver nanoparticles. *RSC Adv* 5: 24513–24520. https://doi.org/10.1039/C4RA17233G
25. Tyavambiza C, Elbagory AM, Madiehe AM, et al. (2021) The antimicrobial and anti-inflammatory effects of silver nanoparticles synthesized from *Cotyledon orbiculata* aqueous extract. *Nanomaterials* 11: 1343. https://doi.org/10.3390/nano11051343
26. Bouafia A, Laouini SE (2020) Green synthesis of iron oxide nanoparticles by aqueous leaves extract of *Mentha pulegium* L.: Effect of ferric chloride concentration on the type of product. *Mater Lett* 265: 127364. https://doi.org/10.1016/j.matlet.2020.127364
27. Bouafia A, Laouini SE, Khelef A, et al. (2020) Effect of ferric chloride concentration on the type of magnetite (Fe_3O_4) nanoparticles biosynthesized by aqueous leaves extract of *Artemisia* and assessment of their antioxidant activities. *J Cluster Sci* 32: 1033–1041. https://doi.org/10.1007/s10876-020-01868-7
28. Yufanyi D, Ondoh A, Foba-Tendo J, et al. (2015) Effect of decomposition temperature on the crystallinity of α-Fe_2O_3 (hematite) obtained from an iron(III)-hexamethylenetetramine precursor. *Am J Chem* 5: 1–9. https://doi.org/10.5923/j.chemistry.20150501.01
29. Lokole PB, Ngombe NK, Motomba DI, et al. (2024) Preparation and characterization of micellar nanoparticles using crude saponins from five Congolese plant species. *PHSA* 2: 100055. https://doi.org/10.1016/j.pscia.2024.100055
30. Abdul MF, Naz F, Jamro HA, et al. (2021) Facile green synthesis of iron oxide nanoparticles using *Phoenix dactylifera* L. seed extract and their antibacterial applications. *J Pharm Res Int* 33: 21–29. https://doi.org/10.9734/jpri/2021/v33i26B31478
31. Leonov NB (2020) Influence of adsorbed metal atoms on light absorption by a fused silica surface. *Opt Spectrosc* 128: 2046–2249. https://doi.org/10.1134/S0030400X20120954
32. Khalaf A, Abu-Dalo D, AlShamaileh E (2024) Synthesis, characterization, and application of Fe_2O_3 nanophotocatalyst for the treatment of various pollutants in aqueous phase: A systematic review. *Sci World J* 2024: 8644322. https://doi.org/10.1155/2024/8644322
33. Aremu OH, Akintayo CO, Naidoo EB, et al. (2021) Synthesis and applications of nanosized zinc oxide in wastewater treatment: A review. *Int J Environ Sci Technol* https://doi.org/10.1007/s13762-020-03069-1
34. Akintayo CO, Aremu OH, Igboama WN, et al. (2021) Performance evaluation of ultraviolet light and iron oxide nanoparticles for the treatment of synthetic petroleum wastewater: Kinetics of COD removal. *Materials* 14: 5012. https://doi.org/10.3390/ma14175012
35. Bolade OP, Adeniyi KO, Williams A, et al. (2021) Remediation and optimization of petroleum hydrocarbons degradation in contaminated water using alkaline activated persulphate. *J Environ Chem Eng* 9: 105801. https://doi.org/10.1016/j.jece.2021.105801

36. Muthukumar B, Duraimurugan R, Parthipan P, et al. (2024) Synthesis and characterization of iron oxide nanoparticles from *Lawsonia inermis* and its effect on the biodegradation of crude oil hydrocarbon. *Sci Rep* 14: 111. https://doi.org/10.1038/s41598-024-61760-6
37. Tran HD, Nguyen DQ, Do PT, et al. (2023) Kinetics of photocatalytic degradation of organic compounds: A mini-review and new approach. *RSC Adv* 13: 25. https://doi.org/10.1039/D3RA01970E
38. Lewinski N, Colvin V, Drezek R (2008) Cytotoxicity of nanoparticles. *Small* 4: 26–49. https://doi.org/10.1002/smll.200700595

AIMS Press